Received 18 November 2024, accepted 9 December 2024, date of publication 11 December 2024,
date of current version 19 December 2024.

Digital Object Identifier 10.1109/ACCESS.2024.3515880

RESEARCH ARTICLE

Distance Analysis in Regular OWC Deployments

ALI MAHBAS, (Member, IEEE), JOHN COSMAS, (Life Senior Member, IEEE), AND HAMED AL-RAWESHIDY, (Senior Member, IEEE)

Department of Electronic and Electrical Engineering, College of Engineering, Design and Physical Sciences, Brunel University of London, UB8 3PH Uxbridge, U.K.

Corresponding author: Ali Mahbas (ali.mahbas@brunel.ac.uk)

This work was supported by the Brunel University of London, U.K.

ABSTRACT For future wireless networks, including 6G, the ability to accurately model and predict network behaviour is essential for meeting stringent quality of service (QoS) requirements. This paper addresses a critical need in future wireless communication systems, particularly for 6G networks, by providing a comprehensive mathematical framework for modelling network geometry in regular cell deployments. Accurate modelling of network geometry is essential for ensuring high QoS and precise localization. While both regular (e.g., square) and irregular (e.g. Poisson Point Process (PPP)) cell-deployment models have been studied, regular deployments, which are crucial for wireless and optical wireless communications (OWC), have received less attention. This paper proposes a mathematical framework to analyse the distance distribution in various regular cell deployments, including line, square, and hexagon configurations. It derives the probability density function (pdf) of the horizontal (2D) and vertical (3D) distances between a user equipment (UE) and the closest node. The framework reveals inaccuracies in previous assumptions made in the literature regarding distance distribution. The exact pdf of the 2D distance between a randomly located UE and the closest node is derived, considering parameters such as inter-node distance and system dimensions (e.g., width). The framework is extended to study the 3D distance, accounting for both fixed and random height differences between the UE and nodes. The coverage probability (CP) is also derived using the proposed framework, providing a more accurate representation of network performance. The results confirm the accuracy of the proposed analysis and compare it with existing works in the literature. The paper highlights that some of assumptions in these works lead to significant errors, such as a 4dB error in signal to noise ratio (SNR) in square deployments. The proposed framework offers a more precise approach to capturing the system characteristics, leading to better network planning and performance optimization.

INDEX TERMS Coverage probability (CP), distance distribution, hexagon deployment, line deployment, optical wireless communications (OWC), regular deployment, signal to noise ratio (SNR), square deployment.

I. INTRODUCTION

Cell deployment models are extensively used to model different cellular networks and optical wireless communications (OWC) in indoor and outdoor environments. Both regular (e.g. square model) and irregular (e.g. passion point process (PPP)) cell-deployment models are used for addressing different aspects such as system design, system performance, localisation and coverage. The irregular cell-deployment model has received significant attention due to its tractability and suitability for some of the practical scenarios [1], [2], [3], [4], [5], [6], [7], [8], [9], [10], [11]. The irregular model is often used to capture some of the randomness in network geometry due to certain infrastructure constraints [12]. However, it is not suitable for all real-world cell deployments [13]. For instance, many real scenarios, such as outdoor and indoor environments (e.g., OWC systems), are more likely to exhibit regular patterns, as these have been proven to offer better performance where infrastructure constraints are relaxed [14], [15]. Although regular deployments are widely popular in literature and system design, limited work has been done to accurately model the distance distribution

The associate editor coordinating the review of this manuscript and approving it for publication was Stefano Scanzio.

and the impact of network geometry on various system aspects. Most papers studying system parameters in regular cell deployments have not precisely captured the effect of network geometry (e.g., distances). They typically rely on simplified models and/or simulations to incorporate the network geometry's impact on system performance. This paper aims to fill this gap by providing an accurate model that captures the effect of network geometry on system performance in different regular deployments.

Most of studies addressing different aspects in wireless communications have used three approaches to model the distances between a UE of interest and the nodes in regular cell deployments. In the first approach, it is assumed that the UE is located at a fixed distance from the serving node [19], [20], [21], [22]. For instance, the authors in [19] highlighted the capabilities of light-fidelity system (Lifi). It was shown that scalability is considered as one of the main features in this system for short and long-range communications when the distance between the transmitter and receiver was assumed to be fixed. In [20], a new access scheme was proposed in which the frequency-division multiple access for the uplink is considered to collect medical data. The performance of the proposed scheme was analysed for a fixed distance (e.g. $3m$) between the receivers and transmitters. In [21], the trade-off between the energy and spectral efficiency was investigated in non-linear orthogonal frequency-division multiplexing (OFDM) system of visible light communications (VLC). The authors tried to capture the impact of different system parameters (e.g. network geometry) on the system performance. However, the distance distribution was not taken into consideration. In [22] the co-channel interference in one and two-dimensional Lifi networks was investigated by taking into consideration the inter-cell distance (d) and field of view (FOV) when the distance between a UE of interest to the serving node is fixed. Although this approach can show the impact of other system parameters on the system performance, it offers very limited insights regarding the locations and network geometry.

In the second approach, simulation tools have been used to address the regular cell-deployments [23], [24], [25], [26], [27], [28], [29], [30], [31], [32], [33], [34]. Different system performance aspects have addressed in regular deployments. For instance, the achievable rate, power allocation, interference management and the channel gain difference have been addressed in the VLC systems [23], [24], [25], [31]. The hybrid Lifi and wireless fidelity (Wifi) networks have also received attention where different aspects have been addressed such as mobility and load balancing [26], [28], [29], [30], and energy efficiency [27]. Furthermore, a system performance comparison between the regular and irregular cell deployments were presented by using simulations to avoid analysis complexity [32], [33], [34]. The drawback of this approach is the modelling limitations, and the results of simulations can sometimes be difficult to interpret, especially if the system's behaviour is highly non-linear or involves many interacting components. It can be challenging to isolate the effects of individual parameters or fully understand the underlying mechanisms. While simulations are used to model complex systems and provide numerical results based on repeated runs or varying conditions, they sometimes fail to clearly present the underlying assumptions. This contrasts with mathematical modelling, where readers can validate the analysis and assumptions made. We recognize that providing mathematical models is not always feasible due to the complexity of analysis. However, our goal is to offer a mathematical model to study one of the key parameters in wireless communication systems—the distance distribution in regular deployments. This model could serve as a foundation for accurately studying various distance-dependent parameters and aspects of wireless communication.

The third approach included making some assumptions regarding the distances to the serving nodes [12], [15], [35], [36], [37], [38]. In these studies, mathematical models were proposed to address number of important aspects in cellular and OWC networks such as the system performance, rate and coverage, optimising the inter-node distance and quality of coverage in regular cell-deployment (mainly hexagon, square or line deployments). However, these studies assumed that the shape of the cell is disc and the probability density function (pdf) of the distance to the closest node is $f_R(r) = 2r/R_{max}^2$ for two-dimensional deployment (hexagon- and square-deployment) [12], [15], [36], [38] and $f_R(r) = 2/R_{max}$ for one-dimensional deployment (line-deployment) [35], [37] where $R_{max} = d/2$ and d is the inter-node distance. Furthermore, [37] assumed that the pdf of R in two-dimensional deployment (hexagon-deployment) is obtained by $f_R(r) = 12r/d^2\sqrt{3}$. Although, these studies addressed either square or hexagon-shaped cells, they assumed that the shape of the cell is a disc when modelling the distances between the UEs and nodes. As a result, the pdf of the distance becomes a linear function. In fact, the pdf of the distance in a regular shape (non circle) is not a linear function as shown in Figure 1. The disc-shaped cell assumption ignores the fact that the UEs can also be located at the cells' edges which may cause misleading information when studying the system performance and system design. UEs located at the edges of cells typically experience performance degradation due to reduced signal strength, increased interference, and inefficient mobility management. Therefore, employing an accurate model is crucial for system design and optimization.

Furthermore, the studies addressing one-dimensional deployment (line-deployment) did not take into consideration the impact of other system parameters on the distribution of the distance. For instance, the width of the environment (w) was not taken into account when deriving the pdf of the distance to the closest node. Ignoring the width of the environment (w) causes inaccuracy regarding the UEs' locations as it will be shown later in this paper.

On the other hand, the three-dimensional (3D) distance, which often refers to the actual spatial separation between

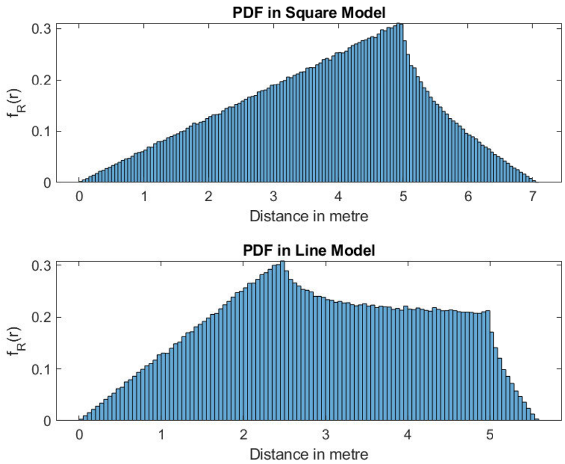

FIGURE 1. Simulation. pdf in square model shows the pdf of the distance between randomly located UE and the nearest node where the node inter-distance (*d*) is 10. pdf in line model shows the pdf of the distance between randomly located UE and the nearest node where the node inter-distance (*d*) is 10 and the width of environment (*w*) is 5.

a transmitter and a receiver considering differences in horizontal and vertical distances, is crucial for calculating signal attenuation and system performance. The 3D distance has often been neglected in wireless communication systems due to the significant difference between cell size and height variation. However, in dense networks and indoor wireless systems (e.g., OWC), the 3D distance cannot be overlooked. This is because considering only the horizontal distance (or two-dimensional (2D) distance) in these environments can significantly affect the accuracy of the analysis [18]. We also believe that any proposed model must account for the characteristics of newly emerged technologies, such as drones. For instance, drones can operate at varying heights, making it crucial to factor in this dimension when evaluating system performance. Some studies [12], [15], [35], [36], [37], [38] have considered 3D distance to analyse system performance, but these analyses were based on the assumption of circular-shaped cells and fixed height difference.

This paper addresses the need for accurate mathematical models to fill the gaps left by existing methods and approaches. Specifically, it proposes a comprehensive mathematical framework that clearly demonstrates the relationship between various system parameters, thereby addressing some of the limitations associated with simulation tools discussed earlier in the paper. Our work also considers future trends in wireless networks, such as high densification, as well as the inclusion of additional system parameters. These trends and parameters have been partially or entirely overlooked in many simplified models found in the literature, leading to potentially misleading conclusions about system performance. In this paper, we propose a framework to derive the pdf of the horizontal distance to the closest node, accounting for actual cell shapes, cell edges, and other system parameters, such as the environment width (w) in line deployments. This framework is further extended to derive the pdf of 3D distance. Additionally, the coverage probability (CP) is derived to illustrate the improvement in modelling accuracy. To ensure accuracy, we derive the exact pdf for 2D distance and extend this to 3D in two scenarios: one where the height of the UE is fixed, and another where height is a random variable. This approach supports various applications and technologies in regular deployments.

The contribution is summarized as follows:

- We propose a framework to study the distribution of the distance between any randomly located user equipment (UE) to the closest node in a regular cell-deployment. An exact pdf of the horizontal distance is derived in a line cell-deployment by taking into consideration that the UEs can be at the cell edges (the cell edges refers to the boundaries or outer limits of cells). This framework also considers other system and environment parameters such as the node inter-distance d, height of UEs h and the width of the environment w.
- Similarly the exact pdf of the horizontal distance between the UE of interest and the closest node is derived in a S-sides cell-deployment (e.g. square, hexagon) where S represents the number of sides that the shape of cell has. For instance, the results become the exact pdf of the distance in square and hexagon shaped-cells if the S parameter is set to 4 and 6 respectively. The results in our paper match the pdf of the distance in the circular-shaped model when assuming the maximum distance between the UE and the closest node is half of the inter-node distance ($d/2$) and the S parameter is ignored. This aligns with the assumptions made in many studies in the literature.
- Due to the importance of the 3D distance in dense and indoor environment, the results are extended to address and derive the exact pdf of the 3D distance between a randomly located UE and the closest node in different regular cell deployments.
- In order to confirm the analysis of this paper and to provide a more accurate representation of network performance in the OWC system, CP is derived by using the proposed framework. CP in OWC system is defined as the probability that the received signal to noise ratio (SNR) at a receiver location is above a certain threshold.

The rest of this paper is structured as follows: Section II describes the system model and derives the pdf of 2D distance in regular deployment models. The pdf of 3D distance is derived in Section III. In Section IV, the coverage probability in OWC system is investigated. The accuracy of our analysis is validated through simulations in Section V. In Section VI, an overview of future research directions is provided. Conclusions are drawn in Section VII.

II. SYSTEM MODEL

Consider UE of interest randomly located within the system. This paper examines the distance distribution in regular cell

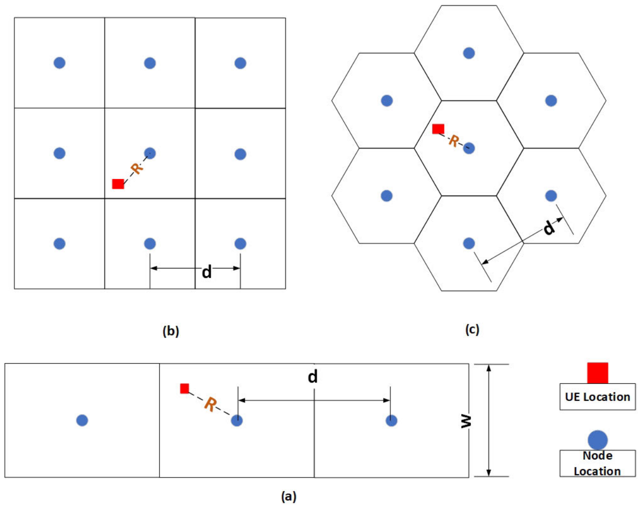

FIGURE 2. Regular deployments. (a) line deployment, (b) square deployment and (c) hexagon deployment.

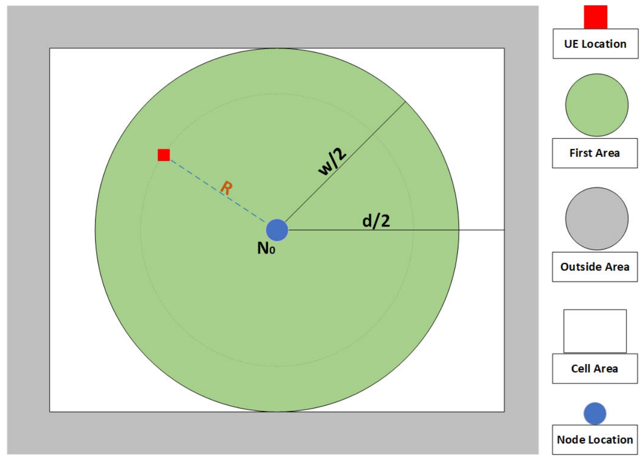

FIGURE 3. Line deployment. First area where UE is located at distance R and $R \leq w/2$.

deployments, focusing on line, hexagonal, and square-shaped cells due to their practical importance. For instance, line deployments are particularly relevant for practical applications such as trains and long corridors (e.g., metro stations, hospitals). We assume that the inter-node distance, which is the distance between any neighbouring nodes, is denoted by d. The width of the environment (e.g., the width of trains or corridors) is represented by w, and the height difference between the level of UEs and the level of nodes in the system is denoted by h, as illustrated in Figure 2. Since the UE is randomly distributed within the system, the distance to the closest node is a random variable. Determining the exact distribution of this distance requires careful consideration of several system parameters. The most relevant parameters include the horizontal distance (2D distance) R, the inter-node distance d, the environment width w, and the height difference h. The horizontal distance R between the UE and the closest node (or the serving cell) can be expressed as:

$$R = \|\mathcal{U} - \mathcal{N}_0\| \tag{1}$$

where $\|.\|$ represents Euclidean distance and, $\mathcal{U}$ and $\mathcal{N}_0$ represent the location of UE and the location of the closest node at the UE's level respectively. The next Definition is used to derive the 2D distance in regular deployment models.

Definition 1: Let $\mathcal{A}$ be the total area of interest and centred at Y. The cumulative distribution function $F_X(x)$ is the probability that a randomly chosen point lies within a radius x. This is the ratio of the total disc area $\mathbb{D}(Y, X)$ inside $\mathcal{A}$ to the total area of interest $\mathcal{A}$:

$$\begin{aligned} F_X(x) &= \mathbb{P}(X \leq x) \\ &= \frac{\mathbb{D}(Y, X) \cap \mathcal{A}}{\mathcal{A}} \end{aligned}$$

where $\mathbb{D}(Y, X)$ is the disc with radius X and centred at Y.

A. LINE MODEL

First, we consider the line deployment where the node inter-distance is represented by d and the width of the system area is represented by w as shown in Figure 2(a). Figure 1, 3, 4 and 5 show that the distance between UE and the closest node $\mathcal{N}_0$ takes any value in the range $(0 \leq R \leq m)$ where $m = \sqrt{d^2/4 + w^2/2}$. Before deriving the pdf of the 2D distance in the line deployment, the distribution of the 2D distance in different areas of the cell needs to be investigated.

Assume that $d > w$, from observation, the cell of interest can be divided into three areas. The first area is where UE located at distance R and $R \leq w/2$ as shown in Figure 3. From Definition 1, the probability of UE being at R distance where $R \leq w/2$ can be interpreted as the ratio of area of the disc $\mathbb{D}(\mathcal{N}_0, R)$ to the total cell area $\mathcal{A}_c$ where $\mathbb{D}(\mathcal{N}_0, R)$ is the disc of radius R and centred at the location of the closest node $\mathcal{N}_0$:

$$\begin{aligned} F_R^{(1)}(r) &= \frac{\mathcal{A}_{1R}(r)}{\mathcal{A}_c} \\ &= \frac{\pi r^2}{\mathcal{A}_c} \quad 0 \leq r \leq \frac{w}{2} \end{aligned} \tag{2}$$

where $\mathcal{A}_c = dw$ is the total area of the cell and $\mathcal{A}_{1R}$ is the area of the disc $\mathbb{D}(\mathcal{N}_0, R)$. UE can also be located in the second area when R is greater than $w/2$ and, equal or smaller than $d/2$ $(w/2 < R \leq d/2)$ as shown in Figure 4. In order to find the distribution of R in the second area of the cell, the outside area $(\mathcal{A}_{O2})$ needs to be obtained. $\mathcal{A}_{O2}$ is defined as the area belongs to the ring $\mathbb{R}(\mathcal{N}_0, w/2, R)$ that does not belong to the area of cell of interest $(\mathcal{A}_c)$, where $\mathbb{R}(\mathcal{N}_0, w/2, R)$ is the area of the ring centred at $\mathcal{N}_0$, $w/2$ is the inner radius, R is the outer radius $(w/2 < R \leq d/2)$.

$$\mathcal{A}_{O2} \in \mathbb{R}(\mathcal{N}_0, w/2, R), \quad \mathcal{A}_{O2} \notin \mathcal{A}_c \tag{3}$$

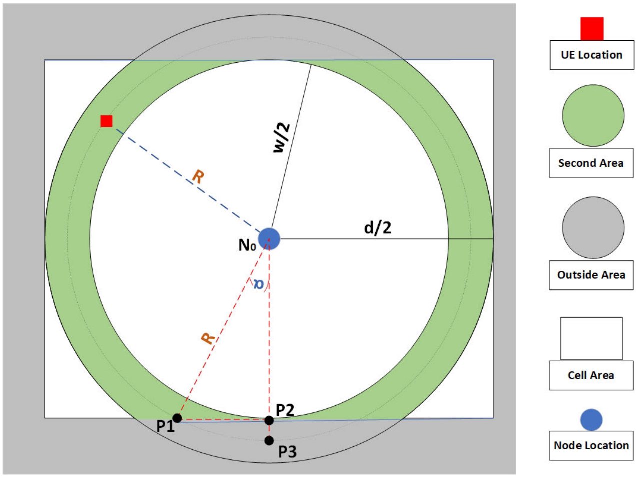

FIGURE 4. Line deployment. Second area where UE is located at distance R and $w/2 < R \leq d/2$.

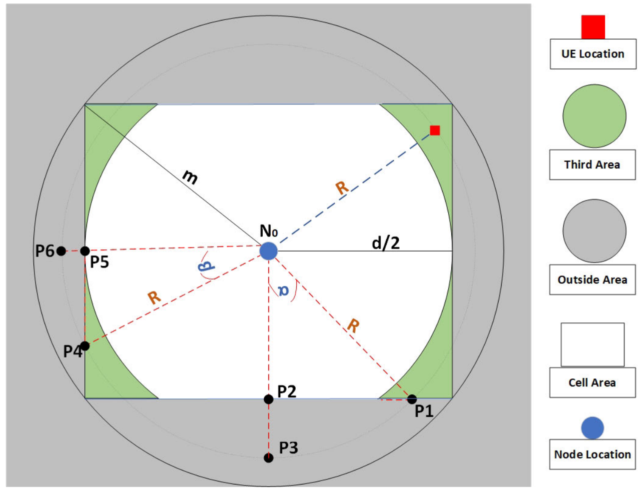

FIGURE 5. Line deployment. Third area where UE is located at distance R and $d/2 < R \leq \sqrt{d^2/4 + w^2/4}$.

Assume a_2 is the area bounded by the points $P1$, $P2$ and $P3$ as shown in Figure 4. a_2 can be obtained by:

$$a_2 = \frac{\alpha \pi R^2}{360} - \frac{w\sqrt{R^2 - \frac{w^2}{4}}}{4} \tag{4}$$

where $\frac{\alpha \pi R^2}{360}$ is the area of sector $\mathbb{S}(\mathcal{N}_0, R, \alpha)$ centred at $\mathcal{N}_0$ with radius R and angle α, $\alpha = \cos^{-1}(\frac{w}{2R})$ obtained from the triangle $\mathbb{T}(\mathcal{N}_0, P1, P2)$ and $\frac{w\sqrt{R^2 - \frac{w^2}{4}}}{4}$ represents the area of triangle $\mathbb{T}(\mathcal{N}_0, P1, P2)$. The outside area $\mathcal{A}_{O2}$ can be found as:

$$\mathcal{A}_{O2} = 4\ a_2 \tag{5}$$

The probability of UE located at distance R where $w/2 < R \leq d/2$ can be obtained by:

$$\begin{aligned} F_R^{(2)}(r) &= \frac{\mathcal{A}_{2R}(r)}{\mathcal{A}_c} \\ &= \frac{\pi r^2 - \mathcal{A}_{O2} - \mathcal{A}_1}{\mathcal{A}_c} \end{aligned} \tag{6}$$

where $\mathcal{A}_1 = \frac{\pi w^2}{4}$ is the maximum value of the first area. Similar to the second area, we need to obtain the outside area $\mathcal{A}_{O3}$ in order to find the probability of UE located in the third area. $\mathcal{A}_{O3}$ is defined as the area belongs to the ring $\mathbb{R}(\mathcal{N}_0, d/2, R)$ that does not belong to the area of cell of interest ($\mathcal{A}_c$), where $\mathbb{R}(\mathcal{N}_0, d/2, R)$ is the area of the ring centred at $\mathcal{N}_0$, $d/2$ is the inner radius, R is the outer radius ($d/2 < R \leq m$) and $m = \sqrt{d^2/4 + w^2/4}$. UE is in the third area at distance R where $d/2 \leq R \leq m$ as shown in Figure 5.

$$\mathcal{A}_{O3} \in \mathbb{R}(\mathcal{N}_0, d/2, R), \mathcal{A}_{O3} \notin \mathcal{A}_c \tag{7}$$

Assume that a_{31} is the area bounded by points $P1$, $P2$ and $P3$ as shown in Figure 5. a_{31} can be obtained by:

$$a_{31} = \frac{\alpha \pi R^2}{360} - \frac{w\sqrt{R^2 - \frac{w^2}{4}}}{4} - \max a_2 \tag{8}$$

where $\frac{\alpha \pi R^2}{360}$ represents the area of sector $\mathbb{S}(\mathcal{N}_0, R, \alpha)$ centred at $\mathcal{N}_0$ with radius R and angle α, $\alpha = \cos^{-1}(\frac{w}{2R})$ obtained from the triangle $\mathbb{T}(\mathcal{N}_0, P1, P2)$ and $\frac{w\sqrt{R^2 - \frac{w^2}{4}}}{4}$ represents the area of $\mathbb{T}(\mathcal{N}_0, P1, P2)$. $\max a_2$ represents the maximum area that a_2 can take. From Eq. (4), a_2 is 0 when $R = w/2$ and it becomes maximum when $R = d/2$. Therefore, $\max a_2$ can be obtained by:

$$\max a_2 = \frac{\cos^{-1}(\frac{w}{d}) \pi d^2}{1440} - \frac{w\sqrt{\frac{d^2}{4} - \frac{w^2}{4}}}{4} \tag{9}$$

Furthermore, a_{32} represents the area bounded by points $P4$, $P5$ and $P6$ as shown in Figure 5. a_{32} can be obtained similar to a_{31}:

$$a_{32} = \frac{\beta \pi R^2}{360} - \frac{d\sqrt{R^2 - \frac{d^2}{4}}}{4} \tag{10}$$

where $\frac{\beta \pi R^2}{360}$ represents the area of sector centred at $\mathcal{N}_0$ with radius R and angle β ($\mathbb{S}(\mathcal{N}_0, R, \beta)$), $\beta = \cos^{-1}(\frac{d}{2R})$ obtained from the triangle $\mathbb{T}(\mathcal{N}_0, P4, P5)$ and $\frac{d\sqrt{R^2 - \frac{d^2}{4}}}{4}$ represents the area of $\mathbb{T}(\mathcal{N}_0, P4, P5)$. The total outside area $\mathcal{A}_{O3}$ can be expressed by:

$$\mathcal{A}_{O3} = 4\ (a_{31} + a_{32}) \tag{11}$$

The probability of UE located at distance R where $d/2 \leq R \leq m$ can be obtained by:

$$\begin{aligned} F_R^{(3)}(r) &= \frac{\mathcal{A}_{3R}(r)}{\mathcal{A}_c} \\ &= \frac{\pi r^2 - \mathcal{A}_{O3} - \mathcal{A}_2 - \mathcal{A}_1}{\mathcal{A}_c} \end{aligned} \tag{12}$$

where $\mathcal{A}_2 = \pi r^2 - \mathcal{A}_{O2} - \mathcal{A}_1$ at $r = d/2$.

The pdf of the distance R in a line cell deployment is obtained in the next Theorem.

Theorem 1: The pdf of the distance between UE and the closest node (R) can be obtained by:

$$f_R(r) = \begin{cases} \frac{2\pi r}{\mathcal{A}_c} & \zeta_1 \\ \frac{1}{\mathcal{A}_c}\left(2\pi r - \frac{\pi r}{45}\cos^{-1}\left(\frac{q}{2r}\right)\right) & \zeta_2 \\ \frac{1}{\mathcal{A}_c}\left(2\pi r - \frac{\pi r}{45}\left(\cos^{-1}\left(\frac{q}{2r}\right)+\cos^{-1}\left(\frac{b}{2r}\right)\right)\right) & \zeta_3 \end{cases} \tag{13}$$

where ζ_1 represents $0 \le r \le \frac{q}{2}$, ζ_2 represents $\frac{q}{2} < r \le \frac{b}{2}$, ζ_3 represents $\frac{b}{2} < r \le m$, $\mathcal{A}_c = qb$, $m = \sqrt{q^2/4 + b^2/4}$, $q = w$ and $b = d$ if $d > w$, and $q = d$ and $b = w$ if $w > d$.

Proof:See Appendix A

B. S-SHAPED MODEL

The two dimensional deployments such as square and hexagon are vital of importance in the other indoor and outdoor applications. Next, S-shaped cells are addressed where S represents the number of sides that each cell has. For instance, in the square deployment model each cell has 4 sides. It is assumed that the all inter-node distance are equal and represented by d. The pdf of distance in cells of S-sided shape is obtained in the next Theorem.

Theorem 2: The pdf of the distance between UE and the closest node (R) in S-sided shape model can be obtained by:

$$f_R(r) = \begin{cases} \frac{2\pi r}{\mathcal{A}_c} & 0 \le r \le \frac{d}{2} \\ \frac{\pi r}{\mathcal{A}_c}\left(4 - \frac{S\cos^{-1}\left(\frac{d}{2r}\right)}{90}\right) & \frac{d}{2} < r \le m \end{cases} \tag{14}$$

where $\mathcal{A}_c = SL_s n/2$ is the total cell area, S is the number of sides that the shape has (e.g. the square has 4 sides and the hexagon has 6 sides), L_s is the length of one side, n is the apothem.

Proof: The pdf of R can be obtained by the derivative of the cdf:

$$f_R(r) = \frac{d}{dr}F_R(r) \tag{15}$$

Consider a square model and similar to line model, the area of the cell can be divided into two areas. For instance, when the node inter-distance is d, the first area forms a disc centred at $\mathcal{N}_0$ with radius of $d/2$. From Definition 1, the probability that UE is located within an area of circle with radius R where $0 \le R \le d/2$ can be expressed as:

$$F_R(r) = \frac{\pi r^2}{\mathcal{A}_c} \tag{16}$$

where $\mathcal{A}_c = d^2$ is the total area of the cell. Furthermore, the UE can also be located in the second area at distance R from the closest node where $d/2 < R \le m$ and m is the distance between the node and any vertex (for instance, $m = d/\sqrt{2}$ when the shape of the cell is square). From Definition 1, the probability that UE located at distance R in the second area is:

$$F_R(r) = \frac{\pi r^2 - \mathcal{A}_1 - A_{O2}}{\mathcal{A}_c} \tag{17}$$

where $\mathcal{A}_1 = \pi d^2/4$, $A_{O2} = 8\ a_2$ and a_2 is obtained similar to Eq. (4). The cdf of R can be represented mathematically:

$$F_R(r) = \begin{cases} \frac{\pi r^2}{\mathcal{A}_c} & 0 \le r \le \frac{d}{2} \\ \frac{\pi r^2 - \mathcal{A}_{O2} - \mathcal{A}_1}{\mathcal{A}_c} & \frac{d}{2} < r \le m \end{cases} \tag{18}$$

the pdf of R is obtained by the derivative of the cdf. When considering S-sided shape model, The results in Eq. (14) is reached. ■

1) SPECIAL CASES

The result in Eq. (14) is the pdf of the distance between a random point and closest node in S-sided model. Below are some of the important special cases for the practical scenarios:

- When $0 \le R \le d/2$, the results represents the pdf of the distance in a cell of circle shape with radius of $d/2$. The pdf of the distance to the closest node is simplified to:

$$f_R(r) = \frac{2\pi r}{\mathcal{A}_c} \tag{19}$$

  where $\mathcal{A}_c = \pi d^2/4$ is the area of the disc. The results in Eq. (19) are equivalent to the pdf of R used by different studies in literature [12], [15], [36], [38].
- When $S = 4$, the results in Eq. (14) represent the pdf of the distance in the square model:

$$f_R(r) = \begin{cases} \frac{2\pi r}{\mathcal{A}_c} & 0 \le r \le \frac{d}{2} \\ \frac{4\pi r}{\mathcal{A}_c}\left(1 - \frac{\cos^{-1}\left(\frac{d}{2r}\right)}{90}\right) & \frac{d}{2} < r \le m \end{cases} \tag{20}$$

  where $\mathcal{A}_c = d^2$ is the area of the cell and $m = d/\sqrt{2}$. Note that the results in Eq. (20) also represent the pdf of distance in line model when $d = w$.
- When $S = 6$, the results in Eq. (14) represent the pdf of the distance in hexagon model:

$$f_R(r) = \begin{cases} \frac{2\pi r}{\mathcal{A}_c} & 0 \le r \le \frac{d}{2} \\ \frac{2\pi r}{\mathcal{A}_c}\left(2 - \frac{\cos^{-1}\left(\frac{d}{2r}\right)}{30}\right) & \frac{d}{2} < r \le m \end{cases} \tag{21}$$

  where $\mathcal{A}_c = 3\sqrt{3}d^2/8$ is the area of the cell and $m = \sqrt{3}d/4$.

Note that the results in (14) represent the distance distribution for any regular shape, including cases where $S > 6$. However, two special cases—when $S = 6$ and

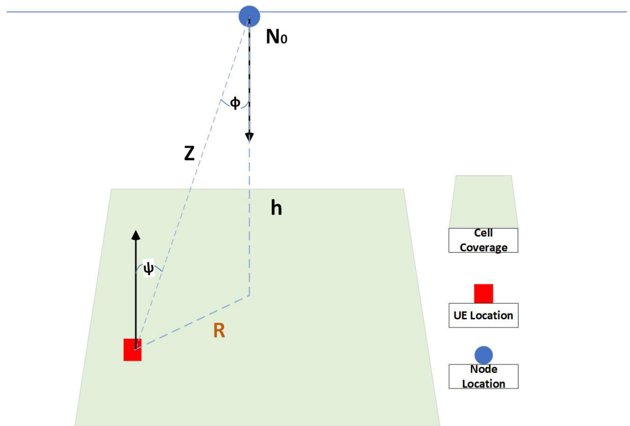

FIGURE 6. **3D distance.**

$S = 4$—are highlighted due to the practical importance of these shapes.

III. 3D DISTANCE

For simplicity, the 3D distance between UE and the nodes is ignored when studying cellular systems due to the significant difference between the cell size and the node height in low density networks. However, the distances to cells are shortened significantly in dense networks. Therefore, it is essential to address the 3D distances when addressing dense networks such as small cells networks and indoor OWC [18]. In this section, the results in the previous section is extended to derive the pdf of 3D distance in regular cell-deployments.

Definition 2: Let X be a random variable with pdf $f_X(x)$. If we have transformation $Y = g(X)$, where g is a function, then the pdf of Y can be found:

$$f_Y(y) = f_X(g^{-1}(y)) \ \left|\frac{d}{dy}g^{-1}(y)\right|$$

where $f_Y(y)$ is the pdf of the transformed random variable Y, g^{-1} is the inverse function of g and $\left|\frac{d}{dy}g^{-1}(y)\right|$ is the absolute value of the derivative of the inverse function evaluated at y.

Theorem 3: The pdf of 3D distance between UE and the closest node in the line model is obtained by:

$$f_Z(z) = \begin{cases} \dfrac{2\pi z}{A_c} & \zeta_1 \\ \dfrac{z\pi}{A_c}\Big(2 - \dfrac{1}{45}\cos^{-1}\left(2\kappa_q\right)\Big) & \zeta_2 \\ \dfrac{z\pi}{A_c}\Big(2 - \dfrac{1}{45}\big(\cos^{-1}\left(\kappa_q\right) + \cos^{-1}\left(\kappa_b\right)\big)\Big) & \zeta_3 \end{cases} \tag{22}$$

where $\kappa_q = \frac{q}{2\sqrt{h^2-z^2}}$, $\kappa_b = \frac{b}{2\sqrt{h^2-z^2}}$, ζ_1 represents $h \leq z \leq \sqrt{h^2 + \frac{q^2}{4}}$, ζ_2 represents $\sqrt{h^2 + \frac{q^2}{4}} < z \leq \sqrt{h^2 + \frac{b^2}{4}}$, ζ_3 represents $\sqrt{h^2 + \frac{b^2}{4}} < z \leq \sqrt{h^2 + \frac{b^2}{4} + \frac{q^2}{4}}$, $q = w$ and $b = d$ if $d > w$, and $q = d$ and $b = w$ if $w > d$.

Proof: See Appendix B

In some scenarios, the height difference between the UEs and nodes is not fixed. For instance, flying drones can be at different heights. Next, the pdf of 3D distance is obtained when the height difference is randomly distributed.

Definition 3: Let $W = g(X, Y)$ be a function of two random variables X and Y with pdf $f_X(x)$ and $f_Y(y)$ respectively. W is also a random variable with pdf of $f_W(w)$ and is obtained by:

$$f_W(w) = \frac{d}{dw}F_w(w)$$

where $F_W(w)$ is the cumulative density function of W and obtained by:

$$\begin{aligned} F_W(w) &= \mathbb{P}(W \leq w) \\ &= \mathbb{P}(g(X, Y) \leq w) \\ &= \int\int f_{X,Y}(x, y)dxdy \end{aligned}$$

where $f_{X,Y}(x, y)$ is the joint pdf of X and Y.

Theorem 4: The pdf of the 3D distance between UE and the closest node when the height difference is a random variable, is obtained by:

$$f_Z(z) = \begin{cases} \dfrac{4\pi z^2}{A_c h_{dif}} & \zeta_1 \\ \dfrac{2\pi z\pi}{A_c h_{dif}}\Big(4z - S\big(\dfrac{z\pi}{2} - \dfrac{2z^2}{d}\mathbb{E}(\sin^{-1}(\dfrac{d}{2z}), \dfrac{d}{2z})\big)\Big) & \zeta_2 \end{cases} \tag{23}$$

where $h_{dif} = h_{max} - h_{min}$, ζ_1 represents $h_{min} \leq z \leq \sqrt{\frac{d^2}{4} + h_{dif}^2}$, ζ_2 represents $\sqrt{\frac{d^2}{4} + h_{dif}^2} < z \leq \sqrt{\frac{d^2}{2} + h_{dif}^2}$, h_{min} is the minimum height, h_{max} is the maximum height and $\mathbb{E}(.)$ is the incomplete elliptic integral of the second kind.

Proof: See Appendix C

IV. COVERAGE PROBABILITY IN OWC

In this section, we use the proposed framework to derive the CP in different deployments of OWC. The CP in an OWC system can be defined as the probability that the received signal to noise ratio (SNR) at a receiver location is above a certain threshold (γ). Mathematically, it can be expressed as:

$$CP = \mathbb{P}(SNR \geq \gamma) \tag{24}$$

where SNR represents the signal to noise ratio and can be calculated by:

$$SNR = \frac{P_t(\mu+1)A_{det}\cos^{\mu}(\phi)\cos(\psi)G_{con}T_s}{2\pi Z^2 NB} \tag{25}$$

where P_t represents the transmitted optical power by individual LED, $\mu = -log_{10}(2)/log_{10}(\cos(\theta))$ is the Lamertian order of emission, θ is the semi-angle at half power, A_{det} is the detector physical area, ϕ and ψ are alignment of the transmitter and receiver, G_{con} is the gain of an optical concentrator, T_s is gain of an optical filter, $Z = \sqrt{R^2 + h^2}$

is the 3D distance between the transmitter and receiver, R is the 2D distance, h is the height difference, B is the system bandwidth, and N is the noise power spectral density. When $\cos(\phi) = \cos(\psi) = h/Z$, the received SNR is expressed by:

$$SNR = \frac{P_t(\mu + 1)A_{det}h^{\mu+1}G_{con}T_s}{2\pi Z^{\mu+3}NB} \tag{26}$$

Incorporating the 3D distance significantly impacts the SNR, especially in dense indoor environments where the height difference between transmitters and receivers can no longer be ignored. This is particularly relevant in scenarios with ceiling-mounted transmitters and ground-level receivers. Ignoring the height difference in such cases can lead to substantial performance discrepancies. The 3D distance affects both the path loss and the received signal strength, as shown in Eq. (26). This can degrade the SNR, coverage, and overall system performance. The error in path loss in dB can be expressed as:

$$\begin{aligned} PL_{error} &= 10\log_{10}\left(Z^{\mu+3}\right) - 10\log_{10}\left(R^{\mu+3}\right) \\ &= 10\Big(\mu + 3\Big)\log_{10}\left(\frac{Z}{R}\right) \\ &= 10\Big(\mu + 3\Big)\log_{10}\left(1 + \left(\frac{h}{R}\right)^2\right) \end{aligned} \tag{27}$$

The final result is derived from the relationship $Z = \sqrt{R^2 + h^2}$. This demonstrates that the path loss error is negligible when R is much larger than h, but becomes significant when R is comparable to h. For instance, if $h/R = 1/10$, the error is as low as 0.15dB. The error increases to 10.8dB when $h/R = 1$. Overlooking the 3D distance leads to an overestimation of the SNR and errors in the overall system performance, particularly in dense and indoor environments. Therefore, CP is obtained by:

$$\begin{aligned} CP &= \mathbb{P}\left(\frac{P_t(\mu + 1)A_{det}h^{\mu+1}G_{con}T_s(BN)^{-1}}{2\pi Z^{\mu+3}} \geq \gamma\right) \\ &= \mathbb{P}\left(Z \geq \left(\frac{2\pi\gamma}{P_t(\mu + 1)A_{det}h^{\mu+1}G_{con}T_s(BN)^{-1}}\right)^{\frac{-1}{\mu+3}}\right) \\ &= F_Z\left(\left(\frac{2\pi\gamma}{P_t(\mu + 1)A_{det}h^{\mu+1}G_{con}T_s(BN)^{-1}}\right)^{\frac{-1}{\mu+3}}\right) \end{aligned} \tag{28}$$

According to Eq. (25), CP is function of Z which is the 3D distance between the UE and serving node. Since Z can be represented in terms of R ($Z = \sqrt{R^2 + h^2}$), CP can be represented in terms of Z as shown in Eq. (28) or in terms of R as shown in Eq. (29):

$$CP = F_R\left(\sqrt{\left(\frac{2\pi\gamma BN}{P_t(\mu + 1)A_{det}h^{\mu+1}G_{con}T_s}\right)^{\frac{-2}{\mu+3}} - h^2}\right) \tag{29}$$

V. RESULTS

The results in this section demonstrate the accuracy of our analysis, along with the impact of various parameters and environmental characteristics. MATLAB is used to simulate the distance distribution in different regular deployments. The environment is assumed to be covered by a grid of cells with regular shapes (square, hexagon, rectangle), as shown in Figure 2. Nodes (or anchors) are located at the centres of the cells at positions $N_1, N_2, \ldots$. The inter-node distance is set to d, the height difference is set to h, and the width of the environment is set to w. The location of the UE is randomly chosen within the system repeatedly, and each time, the distances to the nodes are calculated based on the UE's current position. The distances to all nodes in the system, when the UE and nodes are assumed to be on the same plane ($h = 0$), are denoted as $R_1, R_2, \ldots$, where $R_1 = |\mathcal{U} - N_1|$. The distance to the closest node is given by $R = \min(R_1, R_2, \ldots)$, and the closest node N_0 is the one with the minimum distance (R) to the UE's location. These distances are used to compute and plot the pdf of the distances (both 2D and 3D) in different regular deployments. 2D distances (horizontal or R) are computed from the UE's position to the nodes, ignoring the height difference h, while 3D distances account for the height difference between the UE's and nodes' planes. The 3D distance (Z) is calculated using $Z = \sqrt{R^2 + h^2}$. It is assumed that the physical area of the detector is A_{det}, the optical filter and concentrator gains are T_s and G_{con} respectively, the transmit power for each node is P_t, the semi-angle at half power is θ, the system bandwidth B, and the noise power spectral density is N. The received SNR at the UE's location is calculated using Eq. (26). Note that Sim represents the results obtained from simulations, Exact Form (EF) refers to the results derived using the proposed framework in this paper, and AssumX represents the results based on assumptions made in previous studies when considering X model (note, X takes a value of L, S or H when the model addressed is line, square or hexagon model). The table below summarizes the various parameters used, unless otherwise specified.

Simulation Parameters	
Parameters	Value
Noise power spectral density (N)	$10^{-20}A^2/Hz$
Bandwidth (B)	$20MHz$
Semi-angle at half power (θ)	70°
Transmitted optical power (P_t)	10 Watt
Detector physical area (A_{det})	$10^{-4}m^2$
Gain of optical filter (T_s)	1
Gain of optical concentrator (G_{con})	1
Height difference (h)	$3m$
Corridor width (w)	$2m$
Node inter-distance (d)	$4m$

Figures 7, 8, 9, 10 and 11 show pdf and cdf of the 2D distance to closest node R in the line model when $d > w$, the line model when $w > d$, the square model and the hexagon model. These figures confirm the analysis in this paper and show a comparison between the actual distribution of the 2D distance and some assumptions made in literature. For instance, Figures 7 and 8 show that some papers assume that R has a uniform distribution, however, it is not accurate according to the simulation results. Furthermore, Figures 7

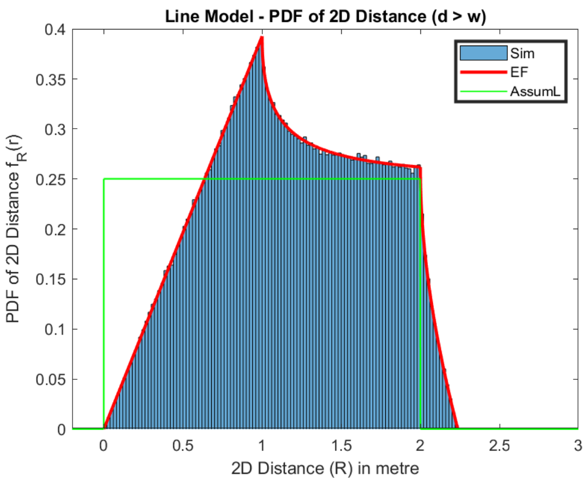

FIGURE 7. The pdf of the 2D distance between UE and nearest node R in line model when $d = 2\ w$. Sim, EF and AssumL represent simulations, exact form (our work) and assumption made by other papers respectively.

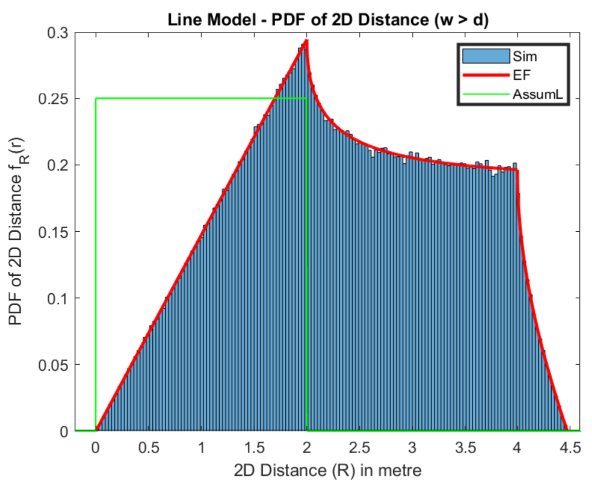

FIGURE 8. The pdf of the 2D distance between UE and nearest node R in line model when $w = 2\ d$. Sim, EF and AssumL represent simulations, exact form (our work) and assumption made by other papers respectively.

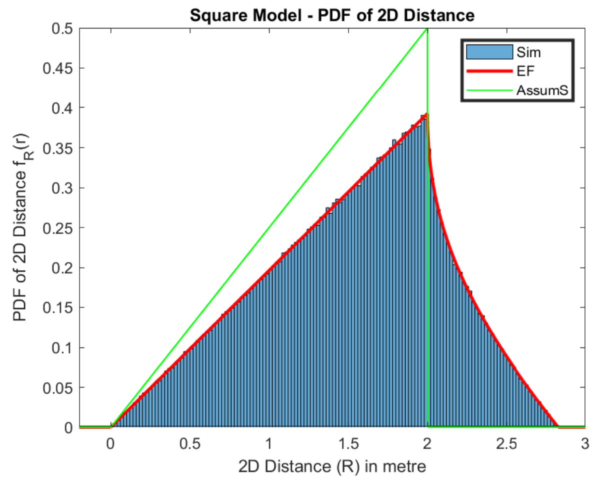

FIGURE 9. The pdf of the 2D distance between UE and nearest node R in square model. Sim, EF and AssumS represent simulations, exact form (our work) and assumption made by other papers respectively.

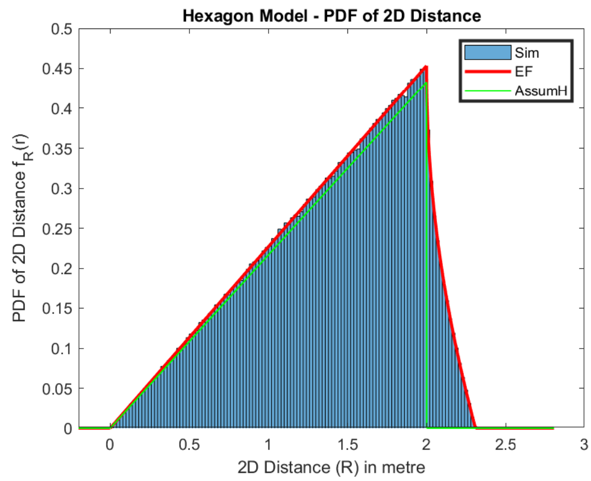

FIGURE 10. The pdf of the 2D distance between UE and nearest node R in hexagon model. Sim, EF and AssumH represent simulations, exact form (our work) and assumption made by other papers respectively.

and 8 show the pdf of R in the line model when $d > w$ and $w > d$ respectively. It can be seen that the distribution of R does not only depend on the inter-node distance (d) but also on the system dimensions such as the width w. Some papers have assumed that the pdf of R is solely a function of d, which is not accurate, as shown in Figures 7 and 8. For instance, Figure 7 shows that the maximum 2D distance is around 2.2 m, while Figure 8 demonstrates that the maximum 2D distance can reach up to 4.5 m. Although the results in both Figures 7 and 8 consider the same inter-node distance ($d = 4$), different values of the environment width are considered: $w = 2$ in Figure 7 and $w = 8$ in Figure 8.

The other drawback of the assumptions made in other studies that the cell's edge is ignored which affect the analysis significantly as shown in Figures 7, 8, 9 and 10. Note that the locations at the cell's edge need more attention as these location are more likely to be subject to performance degradation due to co-channel interference. Ignoring the actual distance distribution and the fact that UEs can be located at the cell's edge, may waste an important opportunity to improve the system performance at the cell's edge. For instance, in Figure 9, the assumptions made in some of the studies addressing square model suggest that the UE can not be at distance greater than $d/2$. However, the simulation and exact form results confirm that the UE can be located at distance greater than $d/2$. Figure 11 shows the cdf of the distance between the UE and the closest node in different deployments. This figure provides a comparison between various deployment types in terms of the expected distance between the UE and its serving cell. It is shown that the 1D deployment (line model) is influenced by the value of w, as explained earlier. Additionally, certain deployments exhibit different distance distributions compared to others.

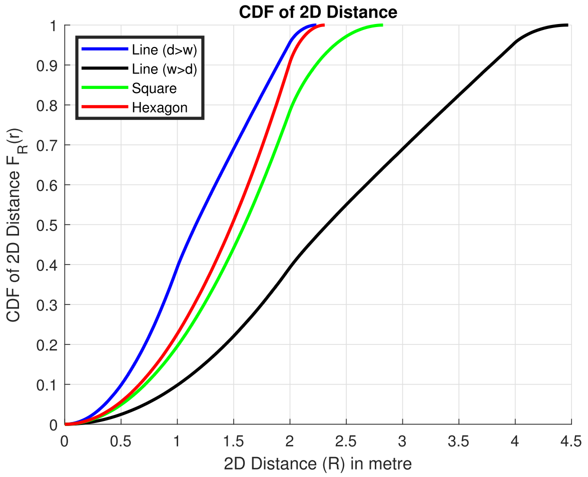

FIGURE 11. The cdf of the 2D distance between UE and nearest node (R) in line model when $d = 2w$, line model when $w = 2d$, square model and hexagon model.

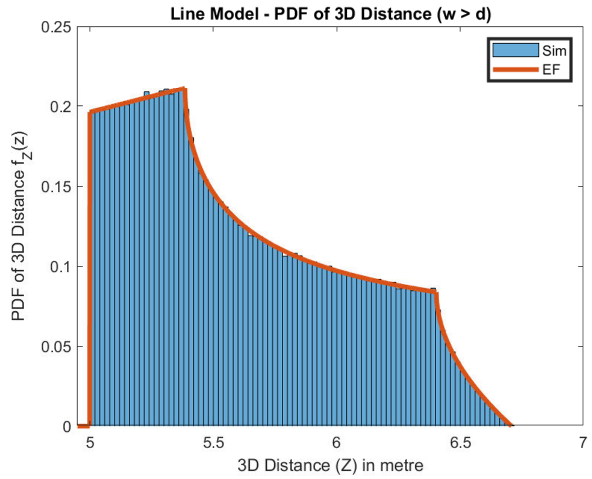

FIGURE 13. The pdf of the 3D distance between UE and nearest node (Z) in line model when $w = 2d$. Sim and EF represent simulations and exact form (our work) respectively.

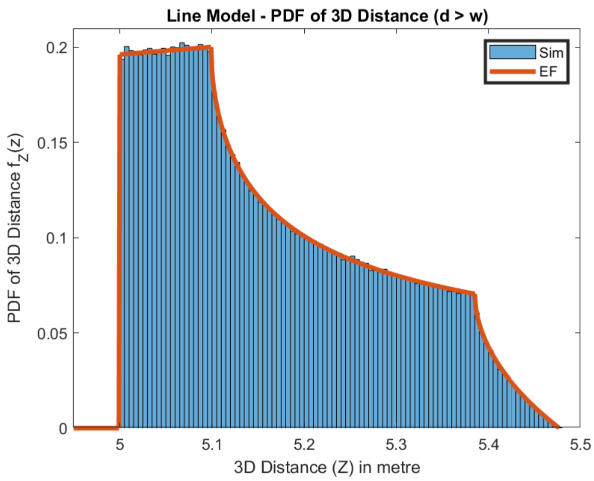

FIGURE 12. The pdf of the 3D distance between UE and nearest node (Z) in line model when $d = 2w$. Sim and EF represent simulations and exact form (our work) respectively.

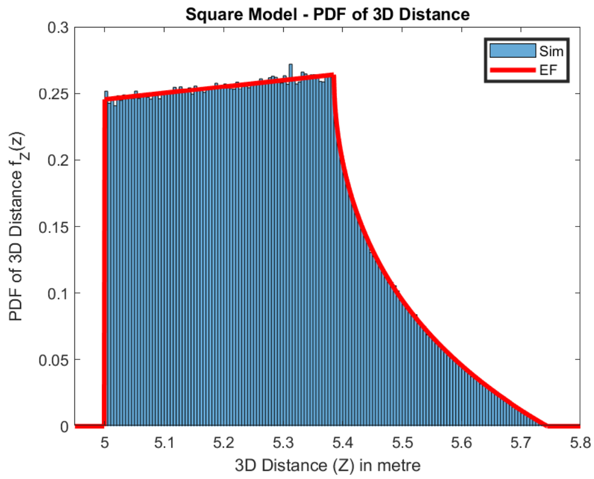

FIGURE 14. The pdf of the 3D distance between UE and nearest node (Z) in square model. Sim and EF represent simulations and exact form (our work) respectively.

For instance, Figures 9, 10 and 11 demonstrates that hexagon deployment can offer shorter distances to nodes compared to other 2D deployments (e.g., square deployment), where the 2D distance in hexagon deployment varies within the range $[0, 2.2]$, while in square deployment, the 2D distance varies within the range $[0, 2.6]$ for the same inter-node distance $d = 4$.

Figures 12, 13, 14, 15, and 16 show the pdf and cdf of the 3D distance between the UE and the closest node in the line model when $d > w$, the line model when $w > d$, the square model, and the hexagon model. These figures also confirm the accuracy of our analysis by comparing the exact form with the simulation results. It can be seen that the distribution of the 3D distance differs from that of the 2D distance due to the height difference. While the height difference can be neglected when the cell area is much larger than the height difference, the results in Figures 12, 13, 14, and 15 show that the height difference must be considered in high-density networks. These figures confirm the analysis presented in this paper, as indicated in Eq. 27, which highlights the importance of incorporating the 3D distance when evaluating system performance, particularly in dense indoor environments where the height difference between transmitters and receivers can no longer be ignored. For instance, the minimum 2D distance is 0 m, and the maximum 2D distances are approximately 2.2 m, 4.5 m, 2.8 m, and 2.3 m in the line model when $d > w$, the line model when $w > d$, the square model, and the hexagon model, respectively, as shown in Figures 7, 8, 9, 10, and 11. However, Figures 12, 13, 14, 15, and 16 show that the minimum 3D distance is 5 m, and the maximum 3D distances are 4.58 m, 6.7 m, 5.7 m, and 5.5 m in the same models. This is due to the significance of the height difference between the UEs and nodes in comparison to the inter-node distance.

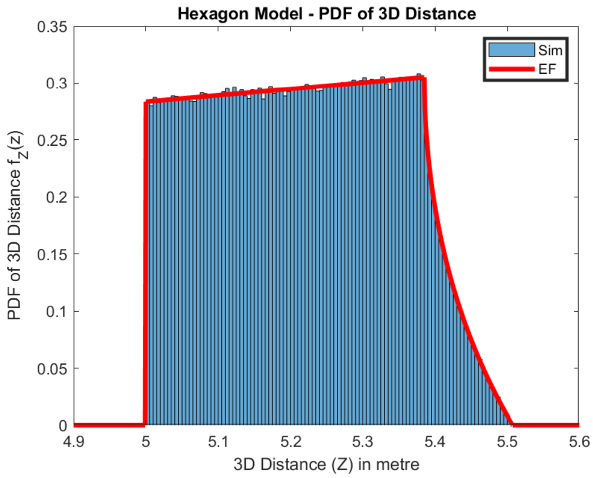

FIGURE 15. **The pdf of the 3D distance between UE and nearest node (Z) in hexagon model. Sim and EF represent simulations and exact form (our work) respectively.**

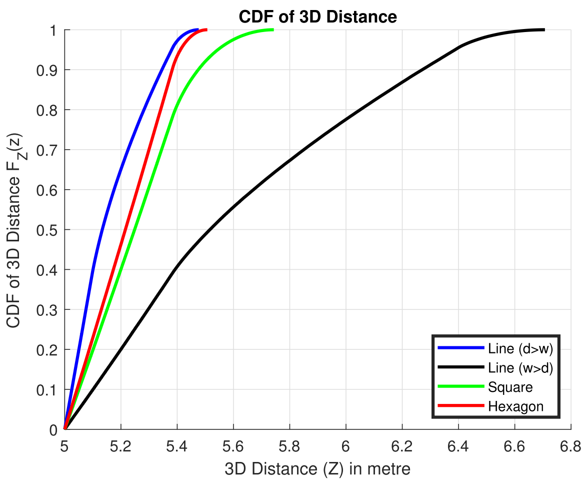

FIGURE 16. **The cdf of the 3D distance between UE and nearest node (Z) in line model when $d = 2\ w$, line model when $w = 2\ d$, square model and hexagon model.**

Moreover, it is demonstrated that certain deployments can offer shorter distances to the nodes or bring the UEs closer to the network. For instance, Figures 14, 15, and 16 show that although the inter-node distance is kept the same, the hexagon deployment provides a shorter distance to the serving cell compared to the square deployment. The maximum distance in the hexagon model is around 5.5 m, while in the square model, it is around 5.75 m for the same inter-node distance ($d = 4$ m). Furthermore, Figures 12 and 13 confirm the importance of considering other system parameters, such as the environment width. The distance distribution is affected when the value of w changes. The maximum 3D distance increases from 5.4 m to 6.7 m when w increases from 2 m to 8 m. Although the environment width has a significant impact on the analysis, it has been ignored in most studies addressing line deployment.

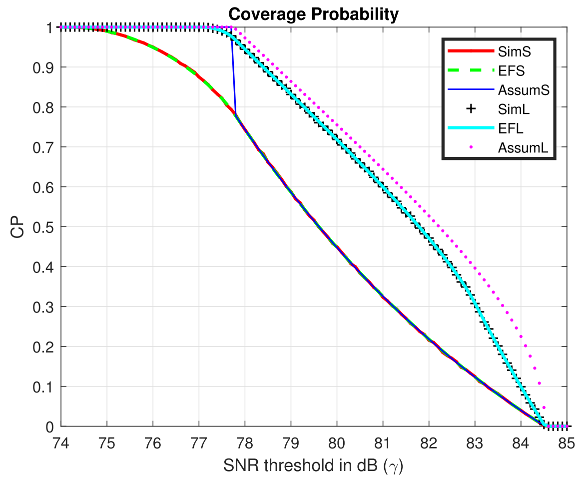

FIGURE 17. **The coverage probability (CP) in 2D deployment (e.g. square) and 1D deployment (line deployment). SimS (SimL), EFS (EFL) and AssumS (AssumL) represent simulations in square deployment (line deployment), our results in square deployment (line deployment) and assumption made by other papers in square deployment (line deployment) respectively.**

Figure 17 presents a comparison of CP between our work and previous studies. This figure shows the CP in two different deployments: 2D deployment (e.g., square deployment) and 1D deployment (e.g., line deployment). The simulation results confirm the accuracy of the analysis in our paper for both deployment types. They also highlight how assumptions made in other studies can impact the accuracy of the results. For instance, in 2D deployment (e.g., square deployment), our findings demonstrate that 100% of the system can achieve 74dB, whereas assumptions made in other studies suggest that 100% of the system can reach nearly 78dB, representing an error of 4dB. These inaccuracies stem from overlooking the distance distribution and the locations at the cell edges. Specifically, these simplified models fail to account for UEs located at the cell edges (i.e., the boundaries or outer limits of cells), where performance degradation occurs due to the increased distance from the node compared to locations closer to the cell centre.

Additionally, our simulations and analysis show a significant error in CP at 78dB, where only 80% of the OWC system can achieve around 78dB. In contrast, simplified models in other studies suggest that 100% of the system can achieve the same performance.

This discrepancy arises because those studies overlook the terminals located at the cells edges or boundaries of cells. Specifically, they fail to accurately model the distance distribution and account for terminals at the cell edges. For example, in 2D deployment (e.g., square model), these studies assume that the UE cannot be located at a distance greater than $d/2$ from the serving cell. In reality, the UE can be situated at a distance greater than $d/2$. Figure 9 shows that according to some literature, the maximum distance the UE can be is 2 m (when $d = 4$). However, our analysis and simulations show that the maximum distance can be around 2.8 m. Furthermore, Figure 11 demonstrates that the probability of the UE being 2 m or less away from the serving cell is around 80%, while the probability of the UE being located more than 2 m away is 20%. Ignoring distances greater than 2 m and the distribution of these distances can overestimate SNR and CP. UEs located at the cell's edge are more likely to experience performance degradation due to their greater distance from the serving cells, resulting in weaker received signal strength.

In contrast, for 1D deployment (or line deployment), studies that addressed this deployment type used simplified models that neglected some important environmental parameters in distance modelling. For instance, the environment width w was not considered in distance distribution modelling. However, Figures 7 and 8 show that this parameter significantly impacts the distance between the UE and the serving cell. These figures also demonstrate that the simplified models become invalid when the environment width w is significant (e.g., in a $w > d$ scenario), as shown in Figure 8, where the maximum distance can reach up to 4.5 m, while the models used in those studies suggest the maximum distance remains 2 m. Since system performance (e.g., SNR and CP) is significantly impacted by the UE's location and network geometry, overlooking the locations of UEs and mischaracterizing the statistical properties of the distances in different deployments will lead to overestimation of SNR and errors in overall system performance, particularly in dense and indoor environments. This is confirmed by Figure 17.

VI. FUTURE RESEARCH

Recognizing the importance of complementing the mathematical framework and simulations with experimental data, the authors are actively exploring opportunities to incorporate practical experiments in future iterations of this work to further validate the performance of OWC systems. The insights and results presented in this paper can also be leveraged to develop more accurate models, thereby enhancing system design and enabling the analysis of various characteristics of different communication networks, including wireless communication and OWC systems, with a focus on mobility management, coverage, and localization. It is important to note that the stringent requirements of future wireless communications pose significant challenges for node deployment and distance measurements in physical setups. Determining the optimal placement of nodes and accurately measuring the distances between UEs and nodes in dense networks is increasingly complex. For example, achieving centimetre- or sub-centimetre-level accuracy in the localization process requires meticulous node deployment and precise distance measurements to minimize errors. However, with careful planning and the use of supporting devices and tools, such as laser pointers and 3D plotters, these challenges can be addressed, thereby improving the accuracy of node and UE placement and the overall reliability of distance measurements in such environments.

Studying the distance distribution within a system is crucial for enhancing performance and avoiding misleading conclusions regarding various distance-dependent factors, such as mobility management and localization. Mobility management significantly impacts user experience and system resource utilization, and it is influenced by network geometry and distance distribution. For instance, when analyzing performance metrics such as handover rate and sojourn time, accurately modelling the movement of UE is essential. The waypoint model has been widely employed for this purpose [16]. In this model, the movement trace of a UE is determined by its starting and destination waypoints, speed, and pause time. Both waypoints are randomly selected within the system, and the UE pauses at the destination point for a specified time. To evaluate system performance (e.g., uplink transmit power and user experience), accurately modelling the distance between the UE and its serving node at these waypoints—and along the path—is vital [11], [17]. Failing to model these distances accurately can lead to errors in mobility management models and misinterpretation of system performance. Moreover, accurately modelling the distance distribution is crucial for the design of localization systems. As demonstrated in [18], the probability of a node providing a Line-of-Sight (LOS) link, which is essential for accurate localization, depends on the characteristics of blockages (e.g., their density and dimensions) and the distance between the node and UE. This highlights the necessity of precise distance modelling to ensure reliable localization and system performance evaluations. The framework we proposed in this paper provides an accurate method for studying the distance distribution between UEs and serving cells in regular deployments, which can be applied to accurately address and model other aspects of the wireless networks. Due to the scope of this paper and the need for careful investigation of other system parameters and scenarios, mobility management and localisation are left for future work.

VII. CONCLUSION

In this paper, the distribution of the distance between a randomly located UE and the closest node in regular deployment models (line, square and hexagon models) is studied. We proposed a new framework to derive the exact form of 2D-distance pdf by taking into consideration the different system parameters such as inter-node distance and the total area of the cell (UE can also located at the cell's edge). The framework was extended to obtain the exact form of 3D-distance pdf when the height difference between the location of UE and the location of the closest node is fixed and random. This is to study different applications and scenarios as the UE can be a drone which may be at different heights. Furthermore, the CP, which is defined as the probability that the received SNR at a receiver location is above a certain threshold, was derived by using the proposed framework. The results confirm the analysis in this paper and show a comparison between the actual distributions of the 2D and 3D distances and some of the assumptions made in literature.

Many of these assumptions are shown to be inaccurate due to significant simplifications and the neglect of crucial system parameters, such as the width of the system in line cell deployments.

Furthermore, it has been demonstrated that accurate modelling of the distance distribution is critical for assessing system performance in OWC systems, particularly in different deployments. Our findings indicate that simplified models used in other studies can lead to significant inaccuracies. For instance, in 2D deployments (e.g., square deployment), our analysis shows an error of 4dB in CP when comparing our accurate model with simplified assumptions. Specifically, while some studies suggest that 100% of the system can achieve nearly 78dB, our results indicate that only 80% of the system can achieve this level, with the rest experiencing weaker performance, especially at the cell edges. This discrepancy stems from the incorrect assumption that UEs cannot be located further than $d/2$ from the serving cell, when in fact UEs can be positioned at greater distances, as demonstrated by our simulations. Similarly, for 1D deployments, we observed that neglecting key environmental factors, such as the width of the deployment area, also leads to significant errors in distance modelling and performance estimation. Our analysis and simulations reveal that the maximum UE distance can exceed the double value of d in wider environments, which is much greater than $d/2$ predicted by some simplified models. The results clearly show that system performance metrics, including SNR and CP, are heavily influenced by the accurate modelling of UE locations (accounting for all potential UE positions within the system, including both the centre and boundaries of the cell) and network geometry. Failure to account for these factors leads to an overestimation of performance, particularly in dense and indoor environments. Our work highlights the importance of using more accurate distance distributions to avoid these errors and better predict real-world system behaviour.

APPENDIX A

The pdf of R can be obtained by the derivative of the cdf:

$$f_R(r) = \frac{d}{dr}F_R(r) \tag{30}$$

when $d > w$, the cdf of R can be interpreted as the probability that $\mathcal{U}$ is inside the disc $\mathbb{D}(\mathcal{N}_0, R)$ of radius R centred at $\mathcal{N}_0$ as noted in Definition 1. From Eq. (2) (Figure 3), Eq. (6) (Figure 4) and Eq. (12) (Figure 5), cdf of R can be represented mathematically:

$$F_R(r) = \begin{cases} \dfrac{\pi r^2}{\mathcal{A}_c} & 0 \le r \le \dfrac{w}{2} \\ \dfrac{\pi r^2 - \mathcal{A}_{O2} - \mathcal{A}_1}{\mathcal{A}_c} & \dfrac{w}{2} < r \le \dfrac{d}{2} \\ \dfrac{\pi r^2 - \mathcal{A}_{O3} - \mathcal{A}_2 - \mathcal{A}_1}{\mathcal{A}_c} & \dfrac{d}{2} < r \le m \end{cases} \tag{31}$$

where $\mathcal{A}_c = wd$, $\mathcal{A}_1 = \pi w^2/4$, $\mathcal{A}_2 = \pi r^2 - \mathcal{A}_{O2} - \mathcal{A}_1$ at $r = d/2$, $\mathcal{A}_{O2}$ is obtained in Eq. (5), $\mathcal{A}_{O3}$ is obtained in Eq. (11). The pdf of R is obtained by the derivative of the cdf of each area of the cell. The pdf of distance in each area becomes:

$$\begin{aligned} f_R^{(1)}(r) &= \frac{d}{dr}F_R^{(1)}(r) \\ &= \frac{d}{dr}\frac{\pi r^2}{\mathcal{A}_c} \\ &= \frac{2\pi r}{\mathcal{A}_c} \qquad 0 \le r \le \frac{w}{2} \end{aligned} \tag{32}$$

$$\begin{aligned} f_R^{(2)}(r) &= \frac{d}{dr}F_R^{(2)}(r) \\ &= \frac{\pi r^2 - \mathcal{A}_{O2} - \mathcal{A}_1}{\mathcal{A}_c} \\ &= \frac{1}{A_c}\Big(2\pi r - \frac{\pi r}{45}\cos^{-1}\big(\frac{w}{2r}\big)\Big) \qquad \frac{w}{2} < r \le \frac{d}{2} \end{aligned} \tag{33}$$

$$\begin{aligned} f_R^{(3)}(r) &= \frac{d}{dr}F_R^{(3)}(r) \\ &= \frac{\pi r^2 - \mathcal{A}_{O3} - \mathcal{A}_2 - \mathcal{A}_1}{\mathcal{A}_c} \\ &= \frac{1}{A_c}\Big(2\pi r - \frac{\pi r}{45}\big(\cos^{-1}\big(\frac{w}{2r}\big) + \cos^{-1}\big(\frac{d}{2r}\big)\big)\Big) \\ &\quad \times \frac{d}{2} < r \le m \end{aligned} \tag{34}$$

The pdf of distance in line deployment when $d > w$ is obtained by:

$$f_R(r) = \begin{cases} \dfrac{2\pi r}{A_c} \\ \dfrac{1}{A_c}\Big(2\pi r - \dfrac{\pi r}{45}\cos^{-1}\big(\dfrac{w}{2r}\big)\Big) \\ \dfrac{1}{A_c}\Big(2\pi r - \dfrac{\pi r}{45}\big(\cos^{-1}\big(\dfrac{w}{2r}\big) + \cos^{-1}\big(\dfrac{d}{2r}\big)\big)\Big) \end{cases} \tag{35}$$

where the limits for the first line is $0 \le r \le \frac{w}{2}$, second line $\frac{w}{2} < r \le \frac{d}{2}$ and third line $\frac{d}{2} < r \le m$. In order to consider different scenarios such as the width of the environment being greater than the inter-node distance $w > d$, parameters q and b are introduced. For instance, q takes the value of w and b takes the value of d when $d > w$. q takes the value of d and b takes the value of w when $w > d$. The results in Eq. (13) is reached.

APPENDIX B

Assume that the height difference between UE and any node is h as shown in Figure 6, hence, the 3D distance to the closest node can be expressed as:

$$Z = \sqrt{R^2 + h^2} \tag{36}$$

Since R is a random variable and its pdf is shown in Theorem 1, Z is also a random variable. The minimum value of Z is h when R is 0, and the maximum value of Z is $\sqrt{h^2+m^2}$ when the 2D distance $R = m = \sqrt{\frac{d^2}{4}+\frac{w^2}{4}}$ is maximum. From Definition 2, the pdf of Z can be obtained by:

$$f_Z(z) = f_R(g^{-1}(z)) \ \left|\frac{d}{dz}g^{-1}(z)\right| \tag{37}$$

where $g^{-1}(z) = \sqrt{z^2-h^2}$ obtained from Eq. (36). From the results in Theorem 1 Eq. (13) and $g^{-1}(z) = \sqrt{z^2-h^2}$, $f_R(g^{-1}(z))$ is expressed by:

$$f_R(g^{-1}(z)) = \begin{cases} \dfrac{2\pi\sqrt{z^2-h^2}}{A_c} \\ \dfrac{\pi}{A_c}\Big(2\sqrt{z^2-h^2} - \dfrac{\sqrt{z^2-h^2}}{45}\cos^{-1}\big(\dfrac{q}{2\sqrt{z^2-h^2}}\big)\Big) \\ \dfrac{\pi}{A_c}\Big(2\sqrt{z^2-h^2} - \dfrac{\sqrt{z^2-h^2}}{45}\big(\cos^{-1}\big(\dfrac{q}{2\sqrt{z^2-h^2}}\big) \\ +\cos^{-1}\big(\dfrac{b}{2\sqrt{z^2-h^2}}\big)\big)\Big) \end{cases} \tag{38}$$

The pdf of Z in Eq. (37) becomes:

$$f_Z(z) = \begin{cases} \dfrac{2\pi\sqrt{z^2-h^2}}{A_c}\bar{g} \\ \dfrac{\pi}{A_c}\Big(2\sqrt{z^2-h^2} - \dfrac{\sqrt{z^2-h^2}}{45}\cos^{-1}\big(\dfrac{q}{2\sqrt{z^2-h^2}}\big)\Big)\bar{g} \\ \dfrac{1}{A_c}\Big(2\pi\sqrt{z^2-h^2} - \dfrac{\pi\sqrt{z^2-h^2}}{45}\big(\cos^{-1}\big(\dfrac{q}{2\sqrt{z^2-h^2}}\big) \\ +\cos^{-1}\big(\dfrac{b}{2\sqrt{z^2-h^2}}\big)\big)\Big)\bar{g} \end{cases} \tag{39}$$

where $\bar{g} = \left|\frac{d}{dz}\sqrt{z^2-h^2}\right|$. when considering the limits for each case, for instance, when $0 \le r \le \frac{q}{2}$, $\frac{q}{2} < r \le \frac{b}{2}$ and $\frac{b}{2} < r \le m$, $h \le z \le \sqrt{h^2+\frac{q^2}{4}}$, $\sqrt{h^2+\frac{q^2}{4}} < z \le \sqrt{h^2+\frac{b^2}{4}}$ and $\sqrt{h^2+\frac{b^2}{4}} < z \le \sqrt{h^2+\frac{b^2}{4}+\frac{q^2}{4}}$. With further simplifications, the final results in Eq. (22) are obtained.

APPENDIX C

Assume that UE can be at any height between h_{min} and h_{max} in Figure 6. The 3D distance between UE and the closest node is obtained by:

$$Z = \sqrt{R^2+H^2} \tag{40}$$

where R is the 2D distance and H is the height difference. Since both R and H are random variables, Z is also a random variable and its pdf can be obtained by using Definition 3.

$$\begin{aligned} F_Z(z) &= \mathbb{P}(Z \le z) \\ &= \mathbb{P}\big(\sqrt{R^2+H^2} \le z\big) \\ &= \int\int f_{R,H}(r,h)drdh \end{aligned} \tag{41}$$

where $f_{R,H}(r,h)$ is the joint pdf. If we assume that R and H are independent, the join pdf becomes:

$$f_{R,H}(r,h) = f_R(r)f_H(h) \tag{42}$$

where $f_R(r)$ is obtained in Eq. (14) when considering 2D deployment (e.g. square or hexagon deployments). Since H can take any value between h_{min} and h_{max}, it is assumed to have a uniform distribution ($f_H(h) = \frac{1}{(h_{max}-h_{min})}$). Thus, the joint pdf ($f_{R,H}(r,h)$) becomes:

$$f_{R,H}(r,h) = \begin{cases} \dfrac{2\pi r}{A_c(h_{max}-h_{min})} \\ \dfrac{\pi r}{A_c(h_{max}-h_{min})}\Big(4 - \dfrac{S}{90}\cos^{-1}(\dfrac{d}{2r})\Big) \end{cases} \tag{43}$$

where A_c represents the cell area, S is the number of sides that each cell has and d is the inter-node distance. The pdf of Z is obtained by:

$$\begin{aligned} f_Z(z) &= \frac{d}{dz}F_Z(z) \\ &\overset{(a)}{=} \frac{d}{dz}\Big(\mathbb{P}\big(z \ge \sqrt{r^2+h^2}\big)\Big) \\ &\overset{(b)}{=} \frac{d}{dz}\Big(\int_{-z}^{z}\int_{-\sqrt{z^2-h^2}}^{\sqrt{z^2-h^2}} f_{R,H}(r,h)drdh\Big) \\ &\overset{(c)}{=} \int_{-z}^{z}\frac{d}{dz}\Big(\int_{-\sqrt{z^2-h^2}}^{\sqrt{z^2-h^2}} f_{R,H}(r,h)dr\Big)dh \\ &\overset{(d)}{=} \int_{-z}^{z}\frac{z}{\sqrt{z^2-h^2}}\Big(f_{R,H}(\sqrt{z^2-h^2},h) \\ &\quad + f_{R,H}(-\sqrt{z^2-h^2},h)\Big)dh \\ &\overset{(e)}{=} \int_{-z}^{z}\frac{z}{\sqrt{z^2-h^2}}f_{R,H}(\sqrt{z^2-h^2},h)dh \end{aligned} \tag{44}$$

where (a) is derived from $F_Z(z) = \mathbb{P}\big(z \ge \sqrt{r^2+h^2}\big)$, (b) follows from Definition 3, with the integral limits obtained from $r = \sqrt{z^2-h^2}$, (c) results from changing the order of integration, (d) is obtained by differentiating the integral limits ($\frac{z}{\sqrt{z^2-h^2}}$) and substituting the integral limits into the joint probability ($f_{R,H}(\sqrt{z^2-h^2},h) + f_{R,H}(-\sqrt{z^2-h^2},h)$), and (e) comes from the fact that $Z \ge 0$. The results in Eq. (23) is reached when solving Eq. (44).

REFERENCES

[1] G. Singh, A. Srivastava, and V. A. Bohara, "Stochastic geometry-based interference characterization for RF and VLC-based vehicular communication system," *IEEE Syst. J.*, vol. 15, no. 2, pp. 2035–2045, Jun. 2021.

[2] J. Kong, M. Ismail, E. Serpedin, and K. A. Qaraqe, "Energy efficient optimization of base station intensities for hybrid RF/VLC networks," *IEEE Trans. Wireless Commun.*, vol. 18, no. 8, pp. 4171–4183, Aug. 2019.

[3] Y. Zhou, N. Huang, and Z. Xu, "Outage and rate analysis for industrial Internet of Things in multitier visible light communication networks inside finite 3-D space," *IEEE Internet Things J.*, vol. 11, no. 11, pp. 20590–20604, Jun. 2024.

[4] A. B. Ozyurt and W. O. Popoola, "LiFi-based D2D communication in industrial IoT," *IEEE Syst. J.*, vol. 17, no. 1, pp. 1591–1598, Mar. 2023.

[5] R. Arshad and L. Lampe, "Stochastic geometry analysis of sojourn time in RF/VLC hybrid networks," *IEEE Trans. Wireless Commun.*, vol. 21, no. 12, pp. 11237–11251, Dec. 2022.

[6] A. B. Ozyurt and W. O. Popoola, "CoMP-JT scheme for D2D communication in industrial LiFi networks," *IEEE Access*, vol. 10, pp. 70760–70768, 2022.

[7] R. Arshad and L. Lampe, "Stochastic geometry analysis of user mobility in RF/VLC hybrid networks," *IEEE Trans. Wireless Commun.*, vol. 20, no. 11, pp. 7404–7419, Nov. 2021.

[8] B. Blaszczyszyn, M. K. Karray, and H. P. Keeler, "Using Poisson processes to model lattice cellular networks," in *Proc. IEEE INFOCOM*, Turin, Italy, Apr. 2013, pp. 773–781.

[9] F. Baccelli and B. Blaszczyszyn, *Stochastic Geometry and Wireless Networks: Volume II Applications*. Boston, MA, USA: Now, 2010.

[10] M. Haenggi, *Stochastic Geometry for Wireless Networks*. Cambridge, U.K.: Cambridge Univ. Press, 2013.

[11] A. J. Mahbas, H. Zhu, and J. Wang, "Impact of small cells overlapping on mobility management," *IEEE Trans. Wireless Commun.*, vol. 18, no. 2, pp. 1054–1068, Feb. 2019.

[12] J. G. Andrews, F. Baccelli, and R. K. Ganti, "A tractable approach to coverage and rate in cellular networks," *IEEE Trans. Commun.*, vol. 59, no. 11, pp. 3122–3134, Nov. 2011.

[13] H. Haas, L. Yin, Y. Wang, and C. Chen, "What is LiFi?" *J. Lightw. Technol.*, vol. 34, no. 6, pp. 1533–1544, Mar. 15, 2016.

[14] M. R. Ghaderi, "LiFi and hybrid WiFi/LiFi indoor networking: From theory to practice," *Opt. Switching Netw.*, vol. 47, Feb. 2023, Art. no. 100699.

[15] C. Chen, D. A. Basnayaka, and H. Haas, "Downlink performance of optical attocell networks," *J. Lightw. Technol.*, vol. 34, no. 1, pp. 137–156, Jan. 1, 2016.

[16] D. B. Johnson and D. A. Maltz, "Dynamic source routing in ad hoc wireless networks," in *Proc. Mobile Comput.*, 1996, pp. 153–181.

[17] A. Mahbas, H. Zhu, and J. Wang, "Trio-connectivity for efficient uplink performance in future mobile HetNets," *IEEE Trans. Veh. Technol.*, vol. 69, no. 12, pp. 15706–15719, Dec. 2020.

[18] A. Mahbas, J. Cosmas, S. Mueen, and J. Wang, "LOS analysis for localization in high frequency systems," *IEEE Trans. Wireless Commun.*, vol. 23, no. 6, pp. 6425–6437, Jun. 2024.

[19] C. Chen, S. Das, S. Videv, A. Sparks, S. Babadi, A. Krishnamoorthy, C. Lee, D. Grieder, K. Hartnett, P. Rudy, J. Raring, M. Najafi, V. K. Papanikolaou, R. Schober, and H. Haas, "100 Gbps indoor access and 4.8 Gbps outdoor point-to-point LiFi transmission systems using laser-based light sources," *J. Lightw. Technol.*, vol. 42, no. 12, pp. 4146–4157, Jun. 15, 2024.

[20] Md. J. Hasan, M. A. Khalighi, V. Jungnickel, L. N. Alves, and B. Béchadergue, "An energy-efficient optical wireless OFDMA scheme for medical body-area networks," *IEEE Trans. Green Commun. Netw.*, vol. 6, no. 3, pp. 1806–1818, Sep. 2022.

[21] Y. Hei, X. Liu, W. Li, S. Wang, and M. Huo, "Energy- and spectral- efficiency tradeoff in nonlinear OFDM system of visible light communications," *J. Lightw. Technol.*, vol. 40, no. 7, pp. 1921–1929, Apr. 1, 2022.

[22] A. Surampudi and R. K. Ganti, "Interference characterization in downlink Li-Fi optical attocell networks," *J. Lightw. Technol.*, vol. 36, no. 16, pp. 3211–3228, Aug. 15, 2018.

[23] L. Qian, X. Chi, L. Zhao, M. Obeed, and A. Chaaban, "User-centric secure cell formation for visible light networks with statistical delay guarantees," *IEEE Trans. Wireless Commun.*, vol. 20, no. 3, pp. 1831–1846, Mar. 2021.

[24] J.-S. Xue, Y.-Y. Zhang, C. Wang, H.-Y. Zhang, and Y.-J. Zhu, "Boundaryless visible light communication system without attocell for industrial Internet of Things," *IEEE Access*, vol. 10, pp. 87454–87460, 2022.

[25] A. Singh, A. Srivastava, V. A. Bohara, and A. K. Jagadeesan, "Optimal LED power allocation framework for a location-assisted indoor visible light communication system," *IEEE Photon. J.*, vol. 14, no. 3, pp. 1–14, Jun. 2022.

[26] G. Ma, R. Parthiban, and N. Karmakar, "An adaptive handover scheme for hybrid LiFi and WiFi networks," *IEEE Access*, vol. 10, pp. 18955–18965, 2022.

[27] M. Asad and S. Qaisar, "Energy efficient QoS-based access point selection in hybrid WiFi and LiFi IoT networks," *IEEE Trans. Green Commun. Netw.*, vol. 6, no. 2, pp. 897–906, Jun. 2022.

[28] X. Wu and D. C. O'Brien, "QoS-driven load balancing in hybrid LiFi and WiFi networks," *IEEE Trans. Wireless Commun.*, vol. 21, no. 4, pp. 2136–2146, Apr. 2022.

[29] Z. Zeng, M. Dehghani Soltani, Y. Wang, X. Wu, and H. Haas, "Realistic indoor hybrid WiFi and OFDMA-based LiFi networks," *IEEE Trans. Commun.*, vol. 68, no. 5, pp. 2978–2991, May 2020.

[30] X. Wu and H. Haas, "Load balancing for hybrid LiFi and WiFi networks: To tackle user mobility and light-path blockage," *IEEE Trans. Commun.*, vol. 68, no. 3, pp. 1675–1683, Mar. 2020.

[31] S. Tao, H. Yu, Q. Li, and Y. Tang, "Derivation and analysis of probability distribution of visible-light channel gain difference based on Lambertian radiation," *IEEE Commun. Lett.*, vol. 24, no. 2, pp. 371–375, Feb. 2020.

[32] A. Guo and M. Haenggi, "Asymptotic deployment gain: A simple approach to characterize the SINR distribution in general cellular networks," *IEEE Trans. Commun.*, vol. 63, no. 3, pp. 962–976, Mar. 2015.

[33] C. S. Chen, V. M. Nguyen, and L. Thomas, "On small cell network deployment: A comparative study of random and grid topologies," in *Proc. IEEE Veh. Technol. Conf. (VTC Fall)*, Sep. 2012, pp. 1–5.

[34] A. Guo and M. Haenggi, "Spatial stochastic models and metrics for the structure of base stations in cellular networks," *IEEE Trans. Wireless Commun.*, vol. 12, no. 11, pp. 5800–5812, Nov. 2013.

[35] M. Kafafy, Y. Fahmy, and M. Khairy, "Optimising the inter-distance between transmitters in a multi-cell VLC system," *IET Commun.*, vol. 13, no. 7, pp. 811–817, Dec. 2018.

[36] J. G. Andrews, F. Baccelli, and R. K. Ganti, "A new tractable model for cellular coverage," in *Proc. 48th Annu. Allerton Conf. Commun., Control, Comput. (Allerton)*, Monticello, IL, USA, Sep. 2010, pp. 1204–1211.

[37] M. Filo, C. H. Foh, S. Vahid, and R. Tafazolli, "Performance analysis of ultra-dense networks with regularly deployed base stations," *IEEE Trans. Wireless Commun.*, vol. 19, no. 5, pp. 3530–3545, May 2020.

[38] J. Li, X. Bao, W. Zhang, and N. Bao, "QoE probability coverage model of indoor visible light communication network," *IEEE Access*, vol. 8, pp. 45390–45399, 2020.

ALI MAHBAS (Member, IEEE) received the B.S. degree in electronic and communication engineering from the University of Technology, Baghdad, Iraq, in 2005, the M.S. degree in communication network planning and management from the University of Portsmouth, U.K., in 2009, and the Ph.D. degree in electronic engineering from the University of Kent, Canterbury, U.K., in 2017. He is currently affiliated with Brunel University London. With over ten years of experience as an Engineer and the Team Leader in telecommunications and mobile networks. His research interests include 6G networks, heterogeneous networks (HetNets), the Internet of Things (IoT), mobility management, localization, optical wireless communications (OWC), orthogonal time frequency space (OTFS) modulation, environmental sensing, and device-to-device communications.

JOHN COSMAS (Life Senior Member, IEEE) received the B.Eng. degree in electronic engineering from Liverpool University, in 1978, and the Ph.D. degree from the Imperial College London, University of London, in 1986.

He is currently a Professor in multimedia systems with the College of Engineering, Design and Physical Sciences, Brunel University London. He is also the Co-Director of the University Research Centre: Intelligent Digital Economy and Society Research Centre (IDEAS). His research interests include the development of multimedia networked systems applied to future of broadcasting, cellular communications, 2D/3D digital video/graphics media and the synergies between these technologies toward their application towards the benefit of the smart homes, cities environment, health, and societies. He has been participating in 16 EU ICT and two EPSRC funded research projects, since 1986, and he has led three of these (CISMUNDUS, PLUTO, and 3D MURALE). He has graduated 36 Ph.D. and four M.Phil. students and published over 91 research journal articles and 200 conference papers. His latest research is concerned with management of heterogeneous cellular networks, convergence of cellular and ad-hoc networks, 3D MIMO, and efficient software defined networks architectures. He can bring 35 years of experience teaching at British universities (Queen Mary University of London and then Brunel University) Digital Electronics and Communications. He has been a BTS Member, since 2006, during which he has actively participated as an Associate Editor of IEEE TRANSACTIONS ON BROADCASTING and annually attend the BTS IEEE Broadband Multimedia Systems and Broadcasting Conference. Through this conference, he has introduced many of his research students and academic colleagues to BTS many of them has subsequently joined the society and made strong contributions as an associate editors, journals, and conference contributors. He has organized an IEEE Broadband Multimedia Systems and Broadcasting Conference, in 2013, in London and a BTS IEEE BTS Young Professionals Conference, in 2019. He is also an Associate Editor of IEEE TRANSACTIONS ON BROADCASTING.

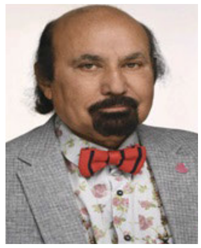

HAMED AL-RAWESHIDY (Senior Member, IEEE) received the Ph.D. degree from Strathclyde University, Glasgow, U.K., in 1991. He is currently a Professor in communications engineering. He was with the Space and Astronomy Research Centre, Iraq, PerkinElmer, USA, Carl Zeiss, Germany, British Telecom, U.K., Oxford University, Manchester Metropolitan University, and Kent University. He is also the Group Leader of the Wireless Networks and Communications Group (WNCG) and the Director of PG studies (EEE) with Brunel University London, U.K. He is also the Co-Director of the Intelligent Digital Economy and Society (IDEAS); the new research center which is a part of the Institute of Digital Futures (IDF). He is also a Course Director for the M.Sc. Wireless Communication and Computer Networks. He is an Editor of the first book in *Radio Over Fiber Technologies for Mobile Communications Networks*. He acts as a Consultant and involved in projects with several companies and operators, such as Vodafone, U.K.; Ericsson, Sweden; Andrew, USA; NEC, Japan; Nokia, Finland; Siemens, Germany; Franc Telecom, France; Thales, U.K. and France; and Tekmar, Italy, Three, Samsung, and Viavi Solutions—actualizing several projects and publications with them. He is also a Principal Investigator for several EPSRC projects and European Project, such as MAGNET EU Project (IP) (2004–2008). He has published more than 500 journals and conference papers. His current research interests include 6G with AI and quantum and the IoT with AI and quantum. He is also an External Examiner of Beijing University for Posts and Telecommunications (BUPT)—Queen Mary University of London. Furthermore, he was an External Examiner for a number of the M.Sc. communications courses with the King's College London, from 2011 to 2016. He has also contributed to several white articles. Specifically, he was an Editor of *Communication and Networking* (White Paper), which has been utilized by the EU commission for research. He has been invited to give presentations at the EU workshop and delivered two presentations at Networld2020 and being the Brunel Representative for NetWorld2020 and WWRF (for the last 15 years).